Kinematic Indicators as Complementary Performance Metrics for PID and Fuzzy Speed Controllers in Rover Actuators

Juan David Guncay , Christian Salamea * , Javier Viñanzaca , Michael Peralta

Posted Date: 9 May 2026

doi: 10.20944/preprints202605.0603.v1

Keywords: control design; linear systems; disturbance rejection (linear case); digital implementation; mechatronic systems; motion control systems

 doi:10.20944/preprints202605.0603.v1

Article

Kinematic Indicators as Complementary Performance Metrics for PID and Fuzzy Speed Controllers in Rover Actuators

Juan Guncay, Christian Salamea *, Javier Viñanzaca and Michael Peralta

Grupo de Investigación en Interacción, Robótica y Automática (GIIRA), Universidad Politécnica Salesiana, Calle Vieja 12-30, Cuenca 010105, Ecuador

* Correspondence: csalamea@ups.edu.ec

Abstract

This work provides an experimental comparison between classical PID, analytically compensated PID, and fuzzy control applied to the speed control of a rover actuator based on a permanent magnet DC motor. Unlike most studies, which focus on classical metrics such as transient response and steady-state error, this work incorporates kinematic indicators such as acceleration and jerk to characterize the dynamic effort applied to the actuator. The results indicate that the fuzzy controller achieves the fastest transient response and the best disturbance rejection, although at the cost of an IAJ 2.378 times higher than that of the classical PID and a peak jerk 79.36% higher under nominal conditions. The classical PID exhibits the smoothest kinematic profile under nominal operation, but under disturbances it generates jerk peaks 2.39 times higher than the fuzzy controller and an IAJ 1.67 times higher than the compensated PID, evidencing its inadequacy under variable loads. The compensated PID achieves the lowest cumulative IAJ under disturbance, outperforming the fuzzy controller by 6.7%, and provides the best overall balance between response speed, disturbance rejection, and cumulative mechanical wear.

Keywords: control design; linear systems; disturbance rejection (linear case); digital implementation; mechatronic systems; motion control systems

1. Introduction

DC motors constitute one of the most relevant elements in a wide variety of modern electromechanical systems, covering applications ranging from consumer electronic devices to industrial systems, mobile robotics, and aerospace platforms [1]. Their persistent relevance compared to other technologies, such as AC motors, is mainly due to their intrinsic characteristics, including high starting torque, an approximately linear relationship between speed and voltage, as well as a notable ease of control stand out [2–9]. These properties make them a particularly attractive alternative in applications where precision, fast response, and simplicity in the implementation of control strategies are required.

In this context, the modeling and dynamic characterization of DC motors are essential for the design of high-performance control systems. The proper identification of dynamic parameters, together with the incorporation of nonlinear phenomena such as Coulomb friction and effects associated with operation under low-voltage regimes, allows a significant improvement in the correspondence between the mathematical model and the real behavior of the system [10,11]. Such fidelity is critical not only for simulation, but also for the effective implementation of control algorithms in physical environments.

In recent years, multiple approaches have been developed aimed at optimizing the performance of DC motors, highlighting the central role of automatic control strategies [12,13]. In particular, speed control has been widely studied, leading to the consolidation of classical techniques such as the proportional-integral-derivative (PID) controller, as well as the development of intelligent approaches, among which fuzzy logic controllers (FLC) stand out. Several works have proposed improvements

 doi:10.20944/preprints202605.0603.v1

over these schemes, including advanced fuzzy control schemes and hybrid PID–FLC configurations with the objective of increasing system robustness and performance [14,15].

Several works have proposed improvements to classical PID controllers through intelligent tuning strategies, including genetic algorithms and particle swarm optimization applied to PMDC motor control [16,17]. Additionally, hybrid configurations combining fuzzy logic with PID structures have been explored, demonstrating improved stability and reduced overshoot compared to classical implementations [18]. Beyond these approaches, alternative control strategies such as optimal control, sliding-mode control, and nonlinear hybrid controllers have been widely investigated to enhance robustness and tracking performance under disturbances and parametric uncertainties [19–23]. However, despite the diversity of control techniques, performance evaluation in most of these studies remains primarily based on classical indicators such as rise time, settling time, steady-state error, and integral error metrics (e.g., IAE, ISE, ITAE), without explicitly considering the kinematic characteristics of the system output.

Despite the abundant existing literature, this predominant reliance on classical transient performance indicators [24–28], particularly in studies focused on PID and fuzzy logic controllers, becomes particularly relevant in real-world applications.

In particular, aspects such as motion smoothness and the mechanical effort induced in actuators are not usually explicitly considered. In this sense, the analysis of kinematic profiles, including variables such as velocity, acceleration, and jerk, acquires significant relevance, since it allows evaluating the impact of the controller on mechanical wear, vibration generation, and system stability under steady-state conditions [29–31]. However, this type of analysis has received limited attention in the literature, highlighting a gap in the comprehensive understanding of controller performance in real-world scenarios.

In response to this problem, this work proposes a comparative analysis of different control strategies applied to a discrete system based on a permanent magnet DC motor (PMDC), integrated into an educational rover-type robot. The main objective is to experimentally evaluate the system's speed control performance, considering not only classical transient response metrics, but also kinematic indicators that enable a more comprehensive characterization of the actuator's dynamic behavior. Three control approaches are implemented and compared: a PID controller tuned using classical methods, a PID controller analytically compensated through pole placement, and a fuzzy controller designed and optimized based on the system's speed and error requirements.

2. Experimental Platform and Embedded Control System

The system under study is the PRAXIA educational robot, a four-wheeled rover-type locomotion platform designed for research in mobile robotics. The platform is depicted in Figure 1, where the wheel arrangement and the distribution of the traction actuation units can be observed.

Each wheel is independently driven by an actuation unit consisting of a PMDC motor and a mechanical support structure. The observable variable of the system is the actuator angular velocity ω, while the control input corresponds to the armature voltage V_a. Both variables are entirely managed within an RP2040 microcontroller, which executes the digital control loop. The general operation scheme is shown in Figure 2.

The angular velocity is estimated from the encoder pulse count within the sampling period Δt. Let N_p denote the number of detected pulses and $\mathcal{R}$ the encoder resolution in pulses per revolution. The angular velocity is computed according to Equation (1):

$$\omega = \frac{N_p}{\mathcal{R}} \cdot \frac{60}{\Delta t} \ [\text{RPM}] \tag{1}$$

For the encoder used in this study, with $\mathcal{R} = 9600$ pulses per revolution. This hardware limitation directly constrains the steady-state behavior of all evaluated controllers.

 doi:10.20944/preprints202605.0603.v1

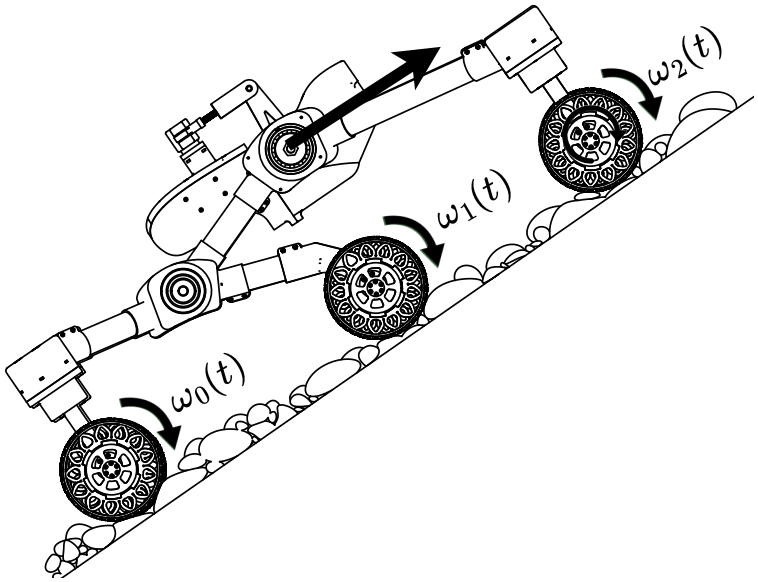

Figure 1. Rover-type mobile robot considered as the application context of the control system.

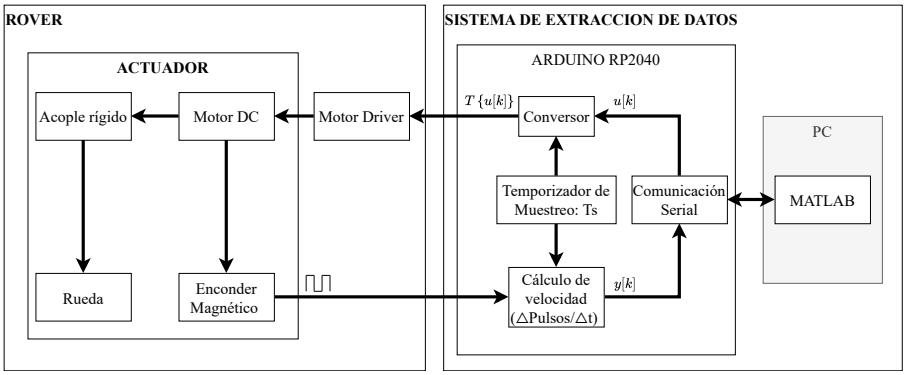

Figure 2. General operation diagram of the actuator control system.

Figure 3 illustrates the implementation architecture within the microcontroller, including the timer-driven execution sequence and the integration of the three evaluated control strategies. This structure ensures homogeneous operating conditions, thereby eliminating potential biases in the experimental comparison. It is worth noting that no filtering is applied to the derivative action, due to the limited encoder resolution. This condition enables the intrinsic behavior of each control strategy to be evaluated under identical hardware constraints.

The actuation unit under study is part of the robot's traction system. It consists of a PMDC motor and a mechanical support structure, as illustrated in Figure 4. The most relevant mechanical interactions for modeling purposes include: the coupling between the motor shaft and the wheel axle, connected through a direct coupling plate, and the bearing assembly, responsible for transmitting and distributing forces between the shaft and the wheel.

 doi:10.20944/preprints202605.0603.v1

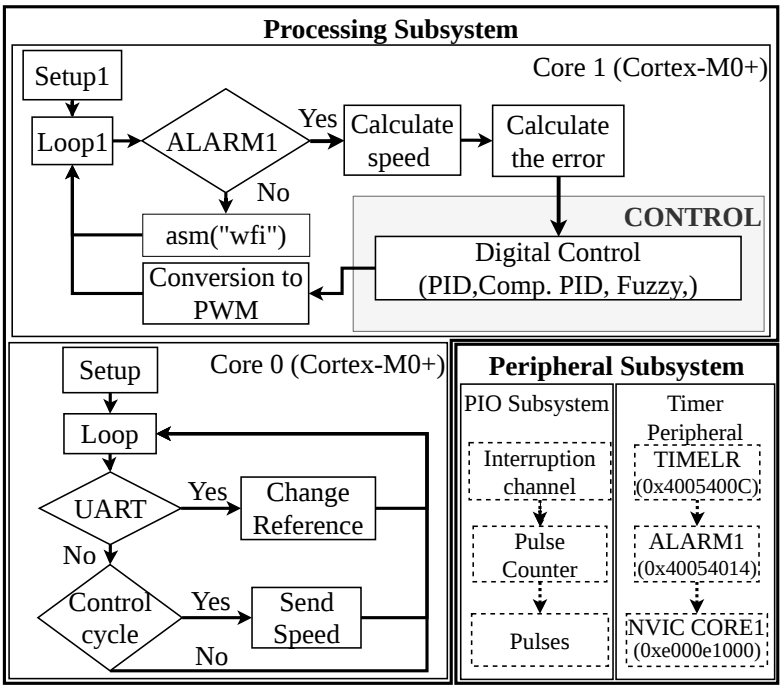

Figure 3. Implementation architecture of the control system on the RP2040 microcontroller.

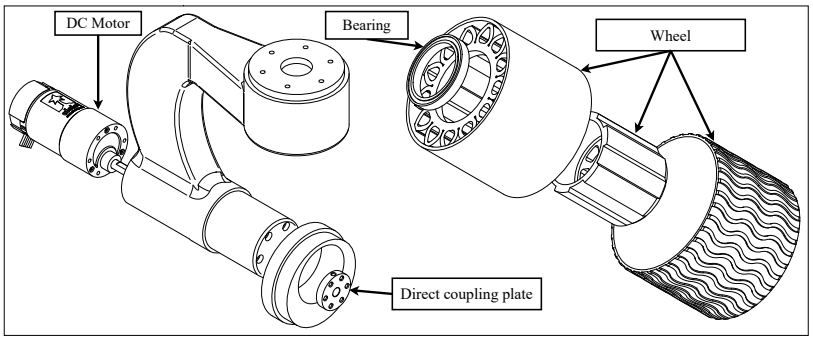

Figure 4. Main mechanical components of the PRAXIA robot actuator.

2.1. System Modeling and Identification

These interactions are jointly represented in the electromechanical model shown in Figure 5, where R and L denote the armature resistance and inductance, respectively; T_d the electromagnetic torque; J_M and J_R the inertia of the motor and the wheel; and B_M and B_R the viscous friction coefficients associated with each component.

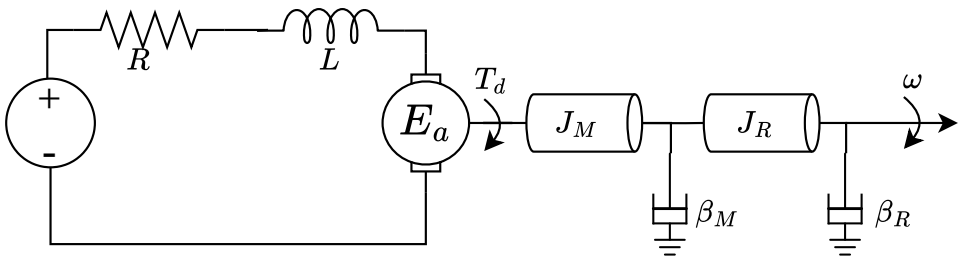

Figure 5. Armature circuit and mechanical representation with coupled load.

 doi:10.20944/preprints202605.0603.v1

With the purpose of reducing the parametric complexity of the model, the inertial and dissipative contributions of the motor and the wheel are merged into equivalent parameters (2) of the system. This grouping is valid assuming a rigid coupling between the motor shaft and the wheel.

$$J = J_M + J_R, \qquad \beta = \beta_M + \beta_R \tag{2}$$

where J represents the total moment of inertia of the system and β the equivalent viscous friction coefficient.

From the electrical and mechanical equations of the DC motor, the second-order state-space model presented in (3) is directly obtained. The state vector is defined as $\mathbf{x} = [x_1 \;\; x_2]^T$, where $x_1 = \omega$ is the angular velocity and $x_2 = \dot{\omega}$ is the angular acceleration, and the system input is the armature voltage $u = V_a$.

$$\dot{\mathbf{x}} = \begin{bmatrix} 0 & 1 \\ -\dfrac{R\beta + K^2}{LJ} & -\dfrac{L\beta + RJ}{LJ} \end{bmatrix} \mathbf{x} + \begin{bmatrix} 0 \\ \dfrac{K}{LJ} \end{bmatrix} u \tag{3}$$

The dynamic behavior of the system is determined by the eigenvalues of the state matrix, obtained from the characteristic polynomial associated with (3). Experimental observations of the motor show that the system operates in an overdamped regime, under which the eigenvalues are real and negative, as expressed in (4).

$$\lambda_{1,2} = \frac{-(L\beta + RJ) \pm \sqrt{(L\beta + RJ)^2 - 4LJ(R\beta + K^2)}}{2LJ} \tag{4}$$

The experimental characterization reveals a marked separation of time scales between both eigenvalues, as expressed in (5).

$$|\lambda_1| = a\,|\lambda_2|, \qquad a \gg 1 \tag{5}$$

Therefore, λ_2 is related to the settling time at 2 % according to (6).

$$\lambda_2 = \frac{-\ln(0.02)}{t_{ss}} \tag{6}$$

2.2. Parametric Identification

For parameter identification, a structural approach based on physical measurements at different steady-state operating levels is adopted, in contrast to black-box methods provided by the MATLAB system identification toolbox, which is used here as a validation reference. The electromotive constant K is estimated through a least-squares fit over the set of measurements, resulting in:

$$K = \frac{\sum_{i=1}^{n} \omega_i V_i - R \sum_{i=1}^{n} \omega_i I_i}{\sum_{i=1}^{n} \omega_i^2} \tag{7}$$

Once K is estimated, the viscous friction coefficient is obtained as:

$$\beta = K \frac{\sum_{i=1}^{n} \omega_i I_i}{\sum_{i=1}^{n} \omega_i^2} \tag{8}$$

Finally, using the relation (6), the equivalent moment of inertia is estimated as:

$$J = \frac{K^2 + \beta R - \beta L \lambda_2}{-L\lambda_2^2 + R\lambda_2} \tag{9}$$

This procedure allows obtaining, in a systematic way and without additional instrumentation, the parameters that cannot be directly measured from the system. The parameterization was carried

 doi:10.20944/preprints202605.0603.v1

out over the six actuators of the robot, obtaining consistent results with small variations. Table 1 summarizes the nominal values and the observed statistical dispersion.

Table 1. Nominal parameters and statistical variability across the 6 actuators.

Parameter	μ	σ ($\pm$)	Units
R	1.95	0.0267	Ω
L	0.0018	0.0002	H
K	1.4010	0.0213	V·s/rad
β	0.0554	0.0025	N·m·s/rad
J	0.0543	0.0017	kg·m^2

Note: The values of σ represent the standard deviation observed across the set of 6 actuators.

2.3. Discretization and Transfer Function

From the mean values and standard deviations obtained in the parametric identification, it is determined that the natural frequency of the actuators lies in the range of 32–33 Hz. Applying the Nyquist criterion with an appropriate safety margin, the selected sampling frequency is $f_s = 100\,\text{Hz}$, corresponding to a sampling period $T_s = 0.01\,\text{s}$.

For the implementation of the digital controller, the continuous state-space model is discretized using zero-order hold (ZOH) with sampling period T_s, obtaining the discrete system:

$$\mathbf{x}[k+1] = A_d\,\mathbf{x}[k] + B_d\,u[k], \qquad \omega_c[k] = C_d\,\mathbf{x}[k] \tag{10}$$

where $C_d = \begin{bmatrix}1 & 0\end{bmatrix}$, $\omega_c[k]$ represents the continuous angular velocity of the actuator, and A_d, B_d are the discrete state and input matrices.

From the eigenvalues λ_1 and λ_2 of the continuous state matrix, the discrete matrices A_d and B_d are, in principle, obtained exactly through the matrix exponential. However, since $|\lambda_1| \gg |\lambda_2|$, the discrete contribution of the fast pole satisfies $e^{\lambda_1 T_s} \approx 1$ under the selected sampling period, which allows simplifying the matrix exponential in the discretization (11) and (12) without compromising dynamic fidelity, as demonstrated through simulation.

$$A_d = \begin{bmatrix} \dfrac{\lambda_1\, e^{\lambda_2 T_s}}{\lambda_1 - \lambda_2} & -\dfrac{e^{\lambda_2 T_s}}{\lambda_1 - \lambda_2} \\[2ex] \dfrac{\lambda_1\lambda_2\, e^{\lambda_2 T_s}}{\lambda_1 - \lambda_2} & -\dfrac{\lambda_2\, e^{\lambda_2 T_s}}{\lambda_1 - \lambda_2} \end{bmatrix}, \tag{11}$$

$$B_d = \begin{bmatrix} -\dfrac{c\lambda_1(e^{\lambda_2 T_s} - 1) + c\lambda_2}{\lambda_1\lambda_2(\lambda_1 - \lambda_2)} \\[2ex] -\dfrac{c\, e^{\lambda_2 T_s}}{\lambda_1 - \lambda_2} \end{bmatrix}. \tag{12}$$

Likewise, for controller design using pole placement, it is convenient to express the model in transfer function form in the z domain, defined as:

$$G(z) = C_d(zI - A_d)^{-1}B_d = \frac{n_1 z + n_0}{z^2 - \text{tr}(A_d)\,z + \det(A_d)}. \tag{13}$$

Since $\det(A_d) = 0$, the denominator factorizes as:

$$z^2 - \text{tr}(A_d)\,z = z\,(z - p), \tag{14}$$

 doi:10.20944/preprints202605.0603.v1

which reveals the presence of a pole at the origin. The transfer function then takes the structural form (15).

$$G(z) = k_m \frac{z + a}{z\,(z - p)}, \tag{15}$$

2.4. Model Validation

Figure 6 compares the proposed physical model with the model obtained through numerical identification in MATLAB. Although the numerical model reduces the error during the transient, the physical model captures the steady-state behavior more accurately, which justifies its selection for controller design.

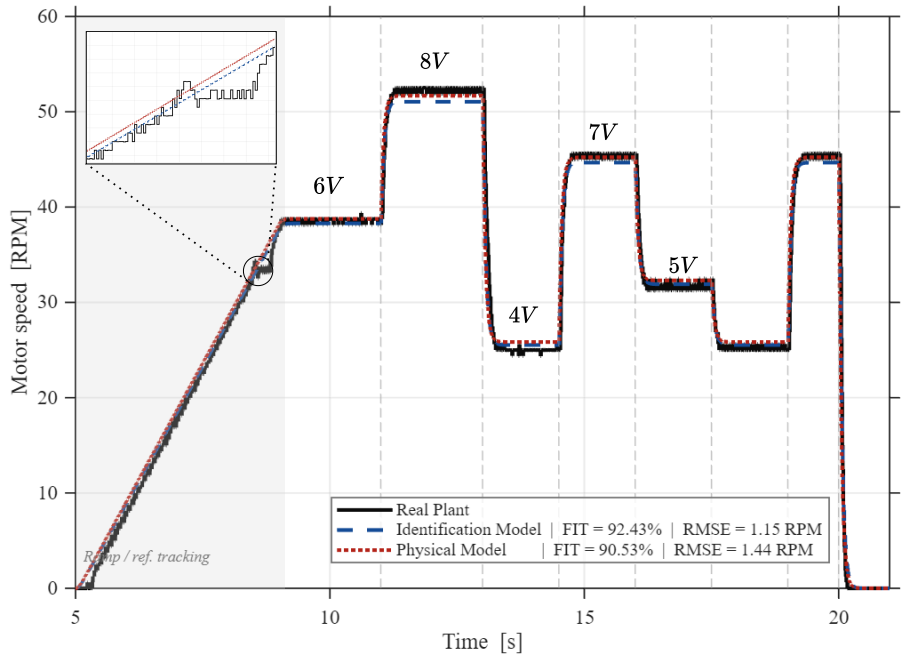

Figure 6. Comparison between the proposed physical model and the numerical identification against the real plant of one of the actuators.

2.5. Encoder Quantization Model

Let $\mathcal{R} = 9600$ be the number of pulses per revolution of the real encoder of the actuator. The minimum speed increment based on Equation (1) is given by:

$$\Delta\omega_c = \frac{2\pi}{\mathcal{R}\,T_s} \tag{16}$$

which, for $T_s = 0.01\,\text{s}$, results in a resolution of $\Delta\omega = 0.0664\,\text{rad/s}$ (0.634 RPM), a limitation that conditions the steady-state behavior of all controllers.

From the estimated continuous velocity $\omega_c[k]$, the equivalent number of encoder increments is computed as an auxiliary variable:

$$n[k] = \frac{\omega_c[k]}{\Delta\omega_c} \tag{17}$$

Decomposing $n[k] = \lfloor n[k] \rfloor + \alpha$, with $\alpha \in [0, 1)$, the integer number of quantized increments $n_q[k]$ is obtained by rounding to the nearest level:

$$n_q[k] = \begin{cases} \lfloor n[k] \rfloor, & \alpha < 0.5 \\ \lfloor n[k] \rfloor + 1, & \alpha > 0.5 \end{cases} \tag{18}$$

 doi:10.20944/preprints202605.0603.v1

In the limiting case $\alpha = 0.5$, a stochastic perturbation is applied to avoid systematic bias:

$$n_q[k] = \lfloor n[k] \rfloor + B, \qquad \mathbb{P}(B = 1) = \tfrac{1}{2} \tag{19}$$

The quantized velocity, delivered to the controller at each sampling cycle, is finally recovered as:

$$\omega[k] = n_q[k] \cdot \Delta\omega_c \tag{20}$$

The measurement resolution is directly conditioned by the sampling period: for $\Delta t = 0.01\,\text{s}$, the obtained resolution is 0.634 RPM, a limitation that must be taken into account in simulation and experimentation.

3. Design and Tuning of Model-Based PID Controllers

From the discrete model, whose dynamics can be represented by a transfer function (15), the design of a speed controller based on a discrete-time PID structure is formulated. Since the plant presents a pole at the origin and a dominant second-order dynamic, it is appropriate to employ control methodologies that allow explicitly imposing the transient behavior of the closed-loop system.

For this purpose, two design strategies are considered: a classical tuning using IMC as a reference, and an analytical tuning based on pole assignment, which directly incorporates the plant dynamics and the desired performance specifications.

3.1. Classical Method

As a reference point, a PID controller is implemented whose parameters are tuned using the PID Tuner tool in MATLAB, taking advantage of the identified dynamic model of the actuator. The overdamped nature of the plant prevents the use of classical empirical methods such as Ziegler–Nichols, whose applicability requires a step response with a well-defined inflection point in the transition region, a condition that the system does not satisfy. The use of PID Tuner therefore allows a systematic tuning based directly on the identified model, under conditions comparable to those of the other evaluated strategies.

This tool employs model-based tuning techniques aligned with the Internal Model Control (IMC) approach, in which the closed-loop performance is specified through a tuning parameter that establishes the trade-off between response speed and robustness [32]. In this way, the variation of this parameter allows adjusting the aggressiveness of the controller in a systematic manner, which provides the tuned PID with quantifiable robustness that can be compared with the other evaluated strategies.

The discrete model of the classical PID controller is given by:

$$u[k] = K_p\, e[k] + K_i\, T_s \sum_{j=0}^{k} e[j] + \frac{K_d}{T_s}\big(e[k] - e[k-1]\big) \tag{21}$$

where $u[k]$ is the control signal and $e[k]$ is the error at sample k. The tuning is carried out with the objective of obtaining a fast response, with reduced overshoot and disturbance rejection capability, prioritizing a stable performance of the robot actuator.

The parameters obtained through the tuning are presented in Table 2.

Table 2. Parameters of the classical PID controller

K_p	K_i	K_d
2.35	15.80	0.012

 doi:10.20944/preprints202605.0603.v1

3.2. *Analytical and Compensated Method*

In order to overcome the limitations of the classical approach, an analytical design method based on pole placement in discrete time is employed. This approach allows incorporating a faster response based on the desired specifications in the closed-loop system.

The controller structure includes two compensation filters, one applied to the error and another to the reference (22).

$$F_e(z) = \frac{z}{z+a},\ F_r(z) = \frac{q_0 + q_1 + q_2}{q_0 z^2 + q_1 z + q_2} \tag{22}$$

The inclusion of these filters allows compensating the controller for its correct operation. The controller is expressed in parametric form through the vectors:

$$\mathbf{q} = \begin{bmatrix} q_0 \\ q_1 \\ q_2 \end{bmatrix}, \quad \mathbf{k_{PID}} = \begin{bmatrix} k_p \\ k_i \\ k_d \end{bmatrix} \tag{23}$$

The design procedure is based on imposing a desired second-order dynamics on the closed-loop system. For this, the desired damping ratio ζ_d and the desired natural frequency ω_d are defined, which determine the parameters:

$$A = e^{-T_s \zeta_d \omega_d},\ B = \cos\left(T_s \omega_d \sqrt{1-\zeta_d^2}\right) \tag{24}$$

From the equality between the desired characteristic polynomial and the denominator of the closed-loop system, the controller coefficients are determined:

$$\mathbf{q} = \frac{1}{k_m} \begin{bmatrix} \epsilon - 2AB + 1 - b \\ A^2 - 2AB\epsilon + b \\ A^2\epsilon \end{bmatrix} \tag{25}$$

corresponds to a non-dominant pole introduced to match both functions, whose dynamics is negligible in the final design.

Once the coefficients $\mathbf{q}$ are obtained, the gains of the discrete PID controller are calculated through the relation:

$$\mathbf{k_{PID}} = \begin{bmatrix} 1 & 0 & -1 \\ T_s^{-1} & T_s^{-1} & T_s^{-1} \\ 0 & 0 & T_s \end{bmatrix} \mathbf{q} \tag{26}$$

This procedure establishes a direct relationship between the desired dynamic specifications and the controller gains, allowing a systematic design based on the plant model. For the considered application, specifications are selected that prioritize a fast response with minimal overshoot, with the objective of avoiding traction losses in the wheels of the system. In particular, a maximum overshoot of 0.1% and a peak time $t_p = 150\,ms$ are established, conditioned by the inherent limitations of the actuator, so that the resulting controller gains are realizable and do not compromise the stability of the system.

The parameters obtained through this procedure are presented in Table 3.

 doi:10.20944/preprints202605.0603.v1

Table 3. Parameters and Gains of the Compensated Discrete PID Controller

Parameter	Symbol	Value
Difference Equation Coefficients		
Coefficient q_0	q_0	3.1687
Coefficient q_1	q_1	-2.3972
Coefficient q_2	q_2	0.0392
PID Controller Gains		
Proportional Gain	k_p	3.1296
Integral Gain	k_i	81.0711
Derivative Gain	k_d	0.00039
Filter Parameter		
Compensation zero	a	0.052

The final structure of the control system is presented in Figure 7, where the compensation filters are integrated with the discrete PID controller.

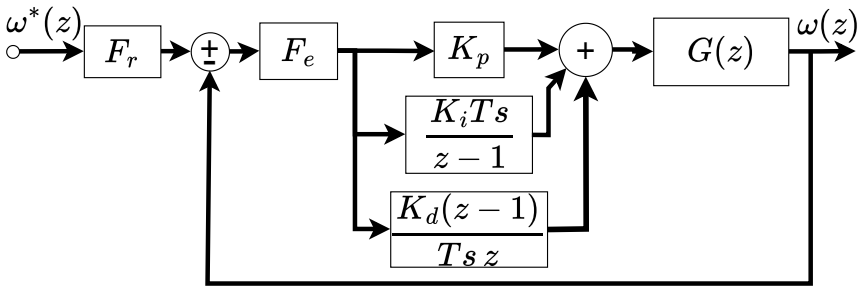

Figure 7. Block diagram of the compensated discrete-time PID control system.

4. Design and Parametric Optimization of a Fuzzy Controller

The fuzzy controller is developed as an alternative to the PID controller, with the objective of evaluating its performance under the same operating conditions, particularly in the presence of disturbances, nonlinearities, and variations in the system dynamics. Unlike the conventional approach, fuzzy control is based on heuristic knowledge, represented through linguistic rules that describe the desired system behavior, whose gains are parametrically optimized to minimize the tracking error based on the obtained model.

The implemented architecture is shown in Figure 8. This structure integrates the computation of the speed error and its derivative with the fuzzy inference system, generating a control variation signal Δu applied to the actuator. The inclusion of the error derivative as an input variable allows the controller to anticipate the dynamic trend of the system, acting in a preventive manner in the presence of imminent changes in speed before the error propagates. In turn, the incremental variation action at the output implicitly introduces an integrating effect in the control signal applied to the actuator, which contributes to reducing the steady-state error.

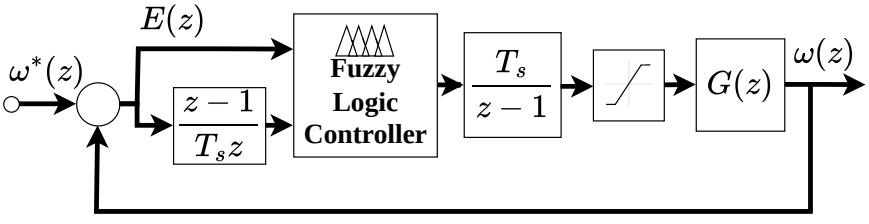

Figure 8. Block representation of the fuzzy control system.

 doi:10.20944/preprints202605.0603.v1

4.1. Input Variables, Universe of Discourse, and Membership Functions

The design of the universe of discourse is based on the physical limitations of the implemented discrete system. As established in Section 2.5, the minimum resolution of the speed measurement from the encoder on the RP2040 microcontroller is 0,0664 rad/s. This value defines the boundary of the system deadband: speed errors below this threshold must be considered as an acceptable region, since they lie within the measurement quantization noise. Consequently, the minimum significant error limit is established, and analogously, the error derivative exhibits the same effective resolution limit, $|\dot{e}_{\min}| = ,065\dot{T}s$ rad/s^2, since it is computed as the difference between consecutive measurements subject to the same quantization.

The membership functions for the input and output variables are illustrated in Figure 9. The inputs e and Δe are classified into seven categories: NG, NM, NP, Z, PP, PM, and PG; analogously, the output ΔV is classified into: VH, MH, H, M, L, ML, and VL, in order to satisfy the system requirements: fast response and minimal overshoot, within the voltage saturation limits of the actuator.

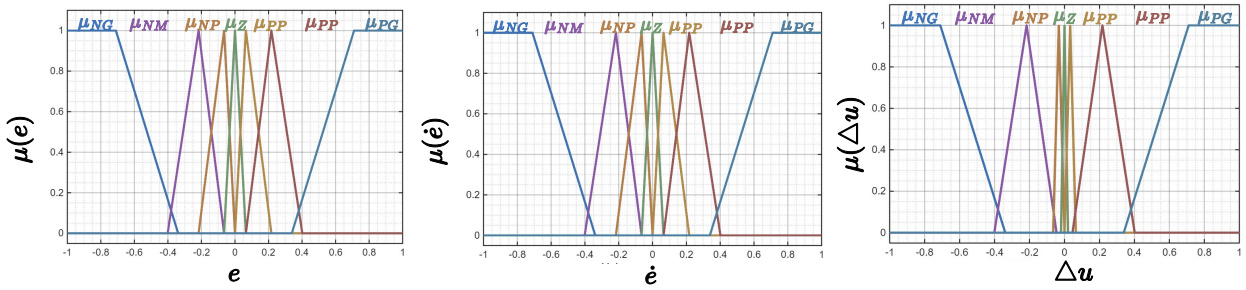

Figure 9. Proposed Fuzzy Logic Controller configuration: (**a**) membership functions of the error input $e(t)$; (**b**) membership functions of the error derivative $\dot{e}(t)$; (**c**) membership functions of the output variable (voltage variation ΔV).

4.2. Inference Rules

The inference rule base, shown in Table 4, was defined according to the specific requirements of the system. A Mamdani-type inference mechanism was employed, with defuzzification using the centroid method.

Table 4. Fuzzy inference rule base for the proposed controller.

$e \setminus \Delta e$	**NG**	**NM**	**NP**	**Z**	**PP**	**PM**	**PG**
NG	VL	VL	VL	VL	VL	ML	ML
NM	VL	ML	ML	L	L	L	H
NP	ML	L	L	L	L	H	H
Z	L	L	L	M	H	H	H
PP	L	L	M	H	H	H	MH
PM	L	M	H	H	MH	MH	VH
PG	H	MH	VH	VH	VH	VH	VH

The design procedure, which includes the selection of input variables, membership functions, their corresponding ranges, and the rule base, was based on configurations reported in previous studies [14,15,24,26,33]. These configurations were adapted to the specific conditions of the system.

Additionally, the type of membership functions was selected considering the feasibility of implementation on a microcontroller operating at a control frequency of 100 Hz.

4.3. Parameterization and Optimization of the Fuzzy Controller

Unlike the PID controller, the fuzzy controller does not have an analytical method that guarantees the effectiveness of the rule base or the membership functions. Therefore, the normalization gains of

 doi:10.20944/preprints202605.0603.v1

the input and output variables (G_e, $G_{\dot{e}}$, G_s) were adjusted using differential evolution, minimizing the cost function defined as:

$$\mathcal{J} = \int_0^2 |e[k]|\, dt \; + \; 0.5\, t_r \; + \; 8 \max\!\left(0,\; \%\overline{OS} - 1\%\right) \tag{27}$$

where t_r is the rise time (10 %–90 %) and $\%OS$ is the percentage overshoot. The search ranges were determined from values reported in the literature. The optimizer was configured with a population size of $N_p = 15$, a convergence tolerance of $\varepsilon = 10^{-7}$, and a fixed seed to ensure reproducibility of the results. The obtained gains are presented below.

Table 5. Controller gains obtained through the optimization process.

G_e	$G_{\Delta e}$	G_s
0.9028	99.434318	238.2141

5. Simulation Framework and Sensitivity Analysis

The simulated response to the step input is presented in Figure 10. The results indicate that the fuzzy controller reaches the reference faster during the transient, followed by the PID compensated by pole placement. The classical PID shows the slowest convergence, with an exponential decay characteristic of its conservative tuning. Regarding the control signal, the classical PID produces the least reactive and lowest-amplitude action, with oscillations attributed to the encoder resolution.

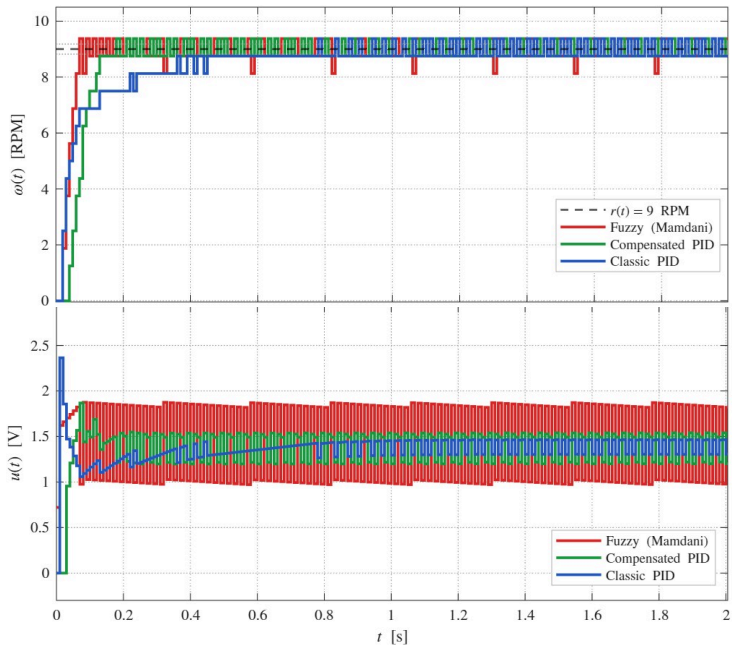

Figure 10. Simulated step response for a reference of 9 RPM

5.1. Parametric Sensitivity Analysis

In order to evaluate the statistical robustness of the comparative results against the manufacturing variability observed among the six rover actuators, a parametric sensitivity analysis was performed using Monte Carlo simulation. For each sample $i \in \{1, \ldots, N_{\mathrm{MC}}\}$, with $N_{\mathrm{MC}} = 500$, a set of perturbed parameters was generated using independent uniform distributions:

$$\theta_i = \theta_0 + \delta_\theta \cdot \varepsilon_i, \quad \varepsilon_i \sim \mathcal{U}(-1, 1), \tag{28}$$

 doi:10.20944/preprints202605.0603.v1

where $\theta \in \{R, L, K, \beta, J\}$, θ_0 denotes the nominal value from Table 1 and δ_θ the corresponding experimentally measured variation bound. For each set θ_i, the matrices $A_d^{(i)}$ and $B_d^{(i)}$ were reconstructed using expressions (11)–(12), and the full simulation described in (10) was executed with the encoder quantization logic according to (20).

The kinematic metrics were evaluated over the steady-state window $t \geq 1$ s, which is sufficient for simulation analysis since the discrete model is deterministic, unlike the experimental environment. Since the angular velocity is obtained from the discrete pulse count of the encoder, the signal exhibits inherent quantization noise, which appears as high-frequency variations in higher-order derivatives. To attenuate this, a Savitzky–Golay filter [34] of order 3 and window length of 21 samples was applied, with a resulting cutoff frequency $f_c = 5.09$ Hz slightly exceeding the tracking loop bandwidth, preserving the transient dynamic trends and removing oscillations of amplitude 0.01–0.06 RPM associated with the finite resolution of the encoder. The same parameterization is used in the processing of experimental data. For each metric $\phi \in \{\text{IAE}, \text{RMS}_j, \text{IAJ}\}$ and each controller c, the sample mean $\bar{\phi}_c$ and standard deviation s_c were estimated according to (29).

$$\bar{\phi}_c = \frac{1}{N_{\text{MC}}} \sum_{i=1}^{N_{\text{MC}}} \phi_c^{(i)}, \qquad s_c = \sqrt{\frac{1}{N_{\text{MC}} - 1} \sum_{i=1}^{N_{\text{MC}}} \left(\phi_c^{(i)} - \bar{\phi}_c\right)^2}, \tag{29}$$

and the coefficient of variation $\text{CV}_c = s_c / \bar{\phi}_c \times 100\,\%$, which quantifies the relative dispersion induced by parametric variability. The ordinal stability of the ranking was evaluated as the fraction of samples in which the cardinal order among controllers is preserved with respect to the nominal case.

The results are summarized in Table 6. The coefficients of variation remained below 1,2 % for the kinematic metrics in the classical PID and the compensated PID, and below 5,2 % for the fuzzy controller, confirming that inter-actuator parametric variability does not significantly alter the absolute performance values. The integral absolute jerk (IAJ) showed a stable ordinal ranking in 100 % of the samples, with the classical PID consistently producing the lowest accumulated dynamic effort ($16{,}54 \pm 0{,}07$ rad/s²), followed by the compensated PID ($16{,}85 \pm 0{,}02$ rad/s²) and the fuzzy controller ($18{,}23 \pm 0{,}94$ rad/s²). The higher coefficient of variation of the fuzzy controller in this metric (CV = 5,17 %) reflects the sensitivity of its nonlinear inference mechanism to variations in the system static gain. In terms of tracking error (IAE), the fuzzy controller achieves the lowest mean value and the ranking is preserved in 87,6 % of the samples,

Table 6. Monte Carlo sensitivity analysis ($N_{\text{MC}} = 500$ samples). Jerk metrics computed via Savitzky–Golay filtering (order 3, window 21) on the steady-state window ($t \geq 1$ s).

Controller	IAE [rad]	RMS j [rad/s^3]	IAJ [rad/s^2]
Classic PID	$0{,}219 \pm 0{,}001$	$14{,}64 \pm 0{,}01$	$16{,}54 \pm 0{,}07$
Comp. PID	$0{,}216 \pm 0{,}000$	$14{,}65 \pm 0{,}02$	$16{,}85 \pm 0{,}02$
Fuzzy Mamdani	$0{,}210 \pm 0{,}008$	$14{,}76 \pm 0{,}17$	$18{,}23 \pm 0{,}94$
CV (%): IAE: 0,27/0,02/3,58; RMS j: 0,04/0,12/1,15; IAJ: 0,40/0,13/5,17 (Classic PID / Comp.PID / FLC).			
IAJ ranking: 100 % stable. IAE ranking: stable in 87,6 % of samples.			

6. Experimental Results and Controller Comparison

The three controllers were implemented directly on the RP2040 microcontroller according to the programming logic described in Figure 3. The experimental validation focuses on a single actuator, selected as the reference unit for having parameters closest to the nominal values in Table 1. This selection is based on the results obtained in the parametric sensitivity analysis. Finally, the step reference profile was selected as the evaluation case, as it is representative of the operating mode. It is worth noting that both the classical PID controller and the compensated PID did not require additional tuning in their implementation in terms of gains; however, the fuzzy controller did require small variations in its gains to operate in a similar manner.

 doi:10.20944/preprints202605.0603.v1

6.1. Unperturbed Condition

This scenario constitutes the baseline reference condition, where the actuator dynamics operate without external disturbances, allowing the intrinsic behavior of each control strategy in the real implementation to be isolated to a greater extent, within the inherent limitations.

6.1.1. Speed Tracking and Transient Response

Figure 11 shows the speed response to step references. The classical PID controller exhibits the slowest transient response. The PID with analytical compensation improves the settling time by explicitly incorporating the identified plant dynamics, and the fuzzy controller achieves the fastest response to the reference change.

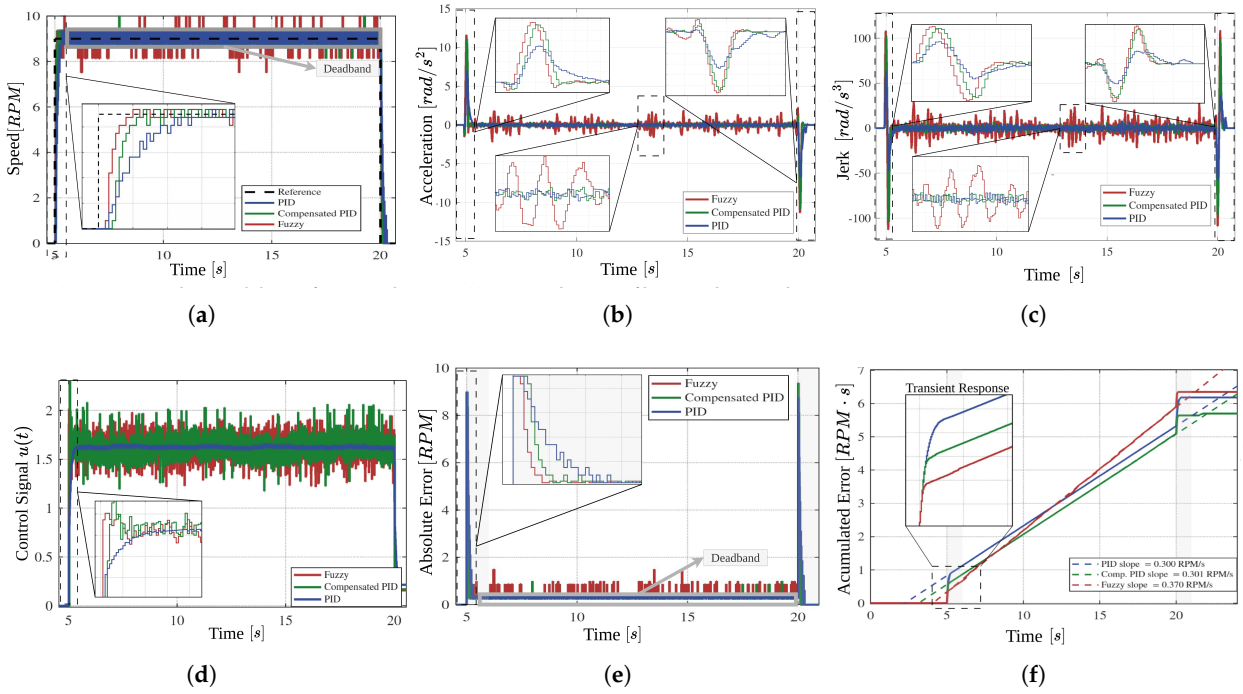

Figure 11. Experimental results for the PMDC motor actuator under disturbance-free conditions: (**a**) speed step response and transient-state behavior; (**b**) acceleration profiles derived via Savitzky–Golay filtering; (**c**) kinematic jerk profiles via derivative smoothing; (**d**) control signal $v(t)$ and actuator effort; (**e**) steady-state absolute error; (**f**) integral of absolute error (IAE) over time.

6.1.2. Steady-State Regime and Control Signal

The steady-state behavior, illustrated in Figure 11e,f, shows a reversal of the ranking with respect to the transient. The fuzzy controller, despite its fast transient response, presents the highest error accumulation rate in steady state, with an approximate slope of $0,37$ RPM/s in the IAE curve. Its reactive nature generates frequent corrections with high variability, while the derivative component of the error, without filtering, amplifies encoder noise and induces residual oscillations instead of stable convergence.

In contrast, the classical PID controller shows the lowest accumulated error slope among the three strategies. Its integral action, of cumulative nature, favors a progressive and sustained convergence to the reference, a behavior that is directly reflected in its control signal (Figure 11d), which is significantly smoother and with lower variability than the other strategies. This characteristic is decisive for prolonged tracking of constant references in a discrete system with quantization noise. The compensated PID occupies an intermediate position: its analytical precompensation attenuates the reactivity to encoder noise compared to the fuzzy controller, but slightly limits the ability to reject small steady-state disturbances compared to the classical PID.

 doi:10.20944/preprints202605.0603.v1

6.1.3. Kinematic Profile and Mechanical Effort Analysis

Figure 11b shows that the fuzzy controller induces the highest acceleration during transients, while the classical PID exhibits the smoothest transitions. The jerk analysis (Figure 11c and Table 7) confirms this trend quantitatively: the fuzzy controller presents an approximate increase of 80% in jerk with respect to the classical PID, measured in peak value, RMS, and integral absolute jerk (IAJ). These indicators are relevant because they reflect the accumulated mechanical effort on the actuator: a high jerk implies abrupt variations in acceleration that generate additional dynamic loads on the bearings, gears, and wheel of the system.

Table 7. Jerk-based performance metrics under no-load conditions (time window: 4–21 s).

Metric	PID	Comp. PID	Fuzzy
Peak $\|j\|$ (rad/s^3)	62.94	104.12	112.89
RMS j (rad/s^3)	7.14	12.00	14.39
IAJ (rad/s^2)	48.69	62.86	115.79
Std Dev j (rad/s^3)	7.14	12.01	14.39
Sign reversals (#)	618	652	312

Overall, the no-load results establish the following trade-off: the fuzzy controller provides the best transient performance but the worst kinematic profile and the highest steady-state error, attributed to its reactive nature without filtering. The classical PID shows the best kinematic profile and the lowest steady-state error accumulation, at the cost of a slower transient response. The compensated PID based on pole placement lies between both strategies.

6.2. Condition with Controlled Disturbances

Controlled disturbances were introduced using a second motor with characteristics identical to the actuator under study, mechanically coupled to the shaft and operated in active braking mode, inducing a tangential force on the wheel and generating a variable disturbance torque. Therefore, the disturbance torque acting on the system can be represented as:

$$T_{\text{dist}} = r \cdot F_{\text{dist}} \tag{30}$$

where r represents the wheel radius of 16 cm, and can be included in the motor mechanical equation as:

$$J\ddot{\theta} = T_d - \beta\dot{\theta} - T_{\text{dist}} \tag{31}$$

which represents the external disturbance torque applied to emulate variable operating conditions on the wheel. The disturbance magnitude was varied by modulating the voltage applied to this load motor, sweeping from 0 % to 100 % of the nominal voltage.

The second evaluation introduces controlled disturbances, with the objective of characterizing the performance of each strategy under nonlinearities and variable loads.

6.2.1. Speed Tracking Under Disturbance

Figure 12a shows that the fuzzy controller maintains its advantage in response speed and is the most effective at attenuating the effects of external disturbances on reference tracking. Its rule-based logic allows it to anticipate the required correction under abrupt load changes, responding more aggressively before the error propagates. The classical PID, in contrast, shows the worst response under disturbances: its conservative tuning was not designed to reject large disturbances, and its relative slowness implies that the system remains in error longer before recovering the reference. The compensated PID significantly improves this behavior with respect to the classical PID, since its pole placement design explicitly imposes the closed-loop dynamics on the identified plant, achieving a more stable and faster convergence under disturbances, although without reaching the anticipation capacity of the fuzzy controller.

 doi:10.20944/preprints202605.0603.v1

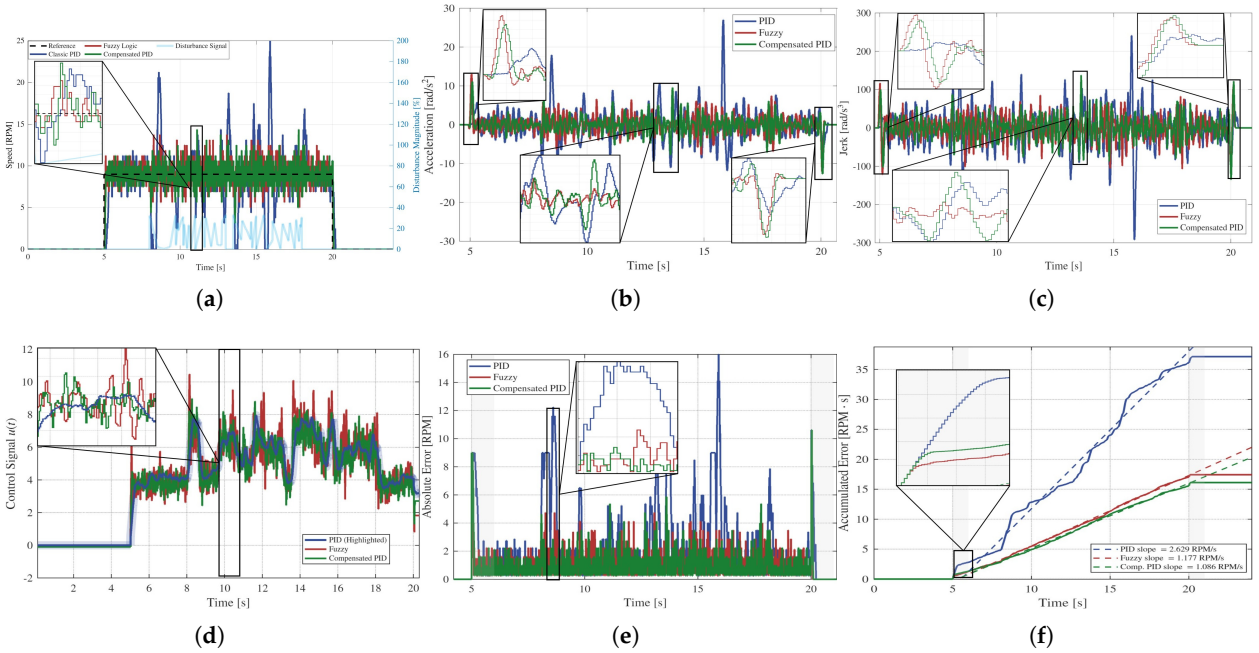

Figure 12. Experimental results for the brushed PMDC motor actuator under perturbation conditions: (**a**) speed step response and transient-state behavior; (**b**) acceleration profiles derived via Savitzky–Golay filtering; (**c**) kinematic jerk profiles via derivative smoothing; (**d**) control signal $v(t)$ and actuator effort; (**e**) steady-state absolute error; (**f**) integral of absolute error (IAE) over time.

However, it is important to note that the higher reactivity of the fuzzy controller under disturbances also implies greater sensitivity to the inherent system noise under steady references, generating low-amplitude oscillations around the operating point that are visible in the speed signal (Figure 12a) during intervals without active disturbance.

6.2.2. Absolute and Accumulated Error Under Load

The analysis of the absolute error (Figure 12e) shows that, under disturbance conditions, the compensated PID achieves the best steady-state performance among the three strategies. Its analytical precompensation, which introduces a delay, acts as an implicit filter for the noise generated by external disturbances, allowing a more precise and sustained correction. The fuzzy controller, although the fastest in the disturbed transient, shows higher variability in the steady reference for the same reason identified in the no-load case: the unfiltered derivative of the error amplifies residual disturbances.

In terms of accumulated error (Figure 12f), the classical PID accumulates approximately 38 RPM · s of absolute error, the worst result among the three strategies, confirming its limited disturbance rejection capability. The fuzzy controller reduces this value due to its fast corrections in disturbed transients, but its steady-state performance limits the total IAE reduction. The compensated PID achieves the best overall result in this metric, maintaining the lowest error accumulation slope, reflecting the most favorable balance between response speed and stability under load.

6.2.3. Kinematic Profile Under Load: Jerk Ranking Inversion

The most relevant result of this section, from the perspective of mechanical wear, is obtained from the combined kinematic analysis of acceleration (Figure 12b), jerk (Figure 12c) and Table 8. Under load conditions, the jerk ranking is inverted with respect to the no-disturbance case: the fuzzy controller now presents the lowest jerk peak (121.94 rad/s^3), compared to the compensated PID (137.44 rad/s^3) and the classical PID (292.01 rad/s^3).

 doi:10.20944/preprints202605.0603.v1

Table 8. Jerk-based performance metrics under load and perturbation conditions.

Metric	PID	Comp. PID	Fuzzy
Peak $\|j\|$ (rad/s^3)	292.01	137.44	121.94
RMS j (rad/s^3)	49.62	29.42	30.67
IAJ (rad/s^2)	590.07	354.22	377.94
Std Dev j (rad/s^3)	49.64	29.43	30.68
Sign reversals (#)	148	228	240

This inversion has a direct physical explanation: under external load disturbances, the classical PID reacts with delay, accumulating error during the disturbance interval and generating a large-amplitude correction when the integral action finally responds, which results in high jerk peaks. The fuzzy controller, in contrast, reacts in advance due to its derivative error component, applying progressive corrections before the error grows in magnitude, resulting in lower acceleration peaks and, consequently, lower peak jerk. This anticipation capability is especially relevant in the rover context, where acceleration peaks can compromise wheel traction on irregular terrain.

However, this advantage of the fuzzy controller must be qualified in the global context of mechanical wear. Although the fuzzy controller presents the lowest jerk peak, the compensated PID achieves lower values in the energy-based metrics (RMS and IAJ), which implies that, over the operating time, the cumulative wear of the compensated PID is lower. This result is consistent with the nature of the fuzzy control signal (Figure 12d): its higher reactivity and correction frequency imply that, although it avoids extreme peaks, it operates with higher sustained activity than the compensated PID, which is reflected in an IAJ that is 6.7% higher.

6.2.4. Comparative Synthesis

Tables 7 and 8, together with the kinematic profiles, allow the definition of three differentiated trade-off profiles. The most relevant result is the complete inversion of the jerk ranking between conditions: under nominal operation, the fuzzy controller produces an IAJ 2.378 times higher than the classical PID and 1.84 times higher than the compensated PID, a penalty attributed to the amplification of quantization noise by its unfiltered derivative action; under disturbance, this relationship is inverted and it is the classical PID that produces the highest accumulated dynamic effort, with an IAJ 1.67 times higher than the compensated PID and 1.56 times higher than the fuzzy controller, as a consequence of its delayed response to variable loads. For peak jerk, the inversion is equally pronounced: the fuzzy controller exceeds the classical PID by 79.36% under nominal condition, while under disturbance the classical PID produces peaks 2.39 times higher than the fuzzy controller and 2.13 times higher than the compensated PID, with direct implications on wheel traction and bearing wear. The compensated PID achieves the lowest cumulative IAJ under disturbance (354.22 rad/s^2), outperforming the fuzzy controller by 6.7 %, which positions it as the strategy with the highest durability in continuous operation. The fuzzy controller is preferable when disturbance rejection and containment of instantaneous peaks are priorities, assuming the cost of a sustained activity 2.38 times higher under nominal condition. The classical PID, although it presents the smoothest kinematic profile without disturbance (IAJ = 48.69 rad/s^2), is not suitable under variable loads where it produces the highest dynamic effort of the set.

7. Conclusions

This work presented an experimental comparison between a classical PID controller, an analytically compensated PID, and a fuzzy controller, implemented directly on an RP2040 microcontroller for the speed control of an actuator in an exploration rover robot. Unlike conventional approaches, the controllers were evaluated in their intrinsic configuration, under the constraints of a discrete embedded implementation.

The results indicate that the fuzzy controller achieved the fastest transient response and the best rejection of peaks under external disturbances; however, in discrete steady-state, its derivative action

 doi:10.20944/preprints202605.0603.v1

amplifies encoder quantization noise, producing a jerk profile 2.378 times higher than that of the classical PID in terms of IAJ and also a peak jerk 79.36% higher, due to its higher reaction speed under nominal conditions. This sustained control activity represents a mechanical cost.

The classical PID showed the smoothest kinematic profile under nominal condition, but its conservative tuning makes it unsuitable under load disturbances, where it produces an IAJ 1.67 times higher than that of the compensated PID and jerk peaks 2.39 times higher than those of the fuzzy controller, as a direct consequence of its delayed response to variable loads. The compensated PID, by explicitly incorporating the identified plant dynamics, achieves the lowest cumulative IAJ under disturbance, outperforming the fuzzy controller by 6.7 %, and thus offers the most favorable balance between response speed, disturbance rejection, and cumulative mechanical wear.

These results show that the inclusion of kinematic indicators such as acceleration and jerk is necessary for a complete evaluation of control strategies in discrete embedded systems: without these metrics, the complete inversion of the dynamic effort ranking between nominal and disturbed conditions would remain unnoticed, leading to incomplete conclusions about the suitability of each strategy for actuator durability in continuous operation.

Author Contributions: Conceptualization, J.G. and C.S.; methodology, J.G. and C.S.; software, J.G. and J.V.; validation, J.G., J.V. and M.P.; formal analysis, J.G. and C.S.; investigation, J.G., J.V. and M.P.; resources, C.S.; data curation, J.V.; writing—original draft preparation, J.G.; writing—review and editing, C.S.; visualization, J.G. and M.P.; supervision, C.S.; project administration, C.S. All authors have read and agreed to the published version of the manuscript.

Funding: This research was funded by Universidad Politécnica Salesiana. The APC was funded by Universidad Politécnica Salesiana.

Institutional Review Board Statement: Not applicable.

Informed Consent Statement: Not applicable.

Data Availability Statement: The raw data supporting the conclusions of this article will be made available by the authors on request.

Acknowledgments: The authors thank the Grupo de Investigación en Interacción, Robótica y Automática (GIIRA) of Universidad Politécnica Salesiana for providing the experimental platform and resources used in this study.

Conflicts of Interest: The authors declare no conflicts of interest. The funders had no role in the design of the study; in the collection, analyses, or interpretation of data; in the writing of the manuscript; or in the decision to publish the results.

References

1. Al-Maliki, A.Y.; Iqbal, K. FLC-based PID controller tuning for sensorless speed control of DC motor. In Proceedings of the Proc IEEE Int Conf Ind Technol. Institute of Electrical and Electronics Engineers Inc., 2018, Vol. 2018-February, pp. 169–174. Journal Abbreviation: Proc IEEE Int Conf Ind Technol, https://doi.org/10.1109/ICIT.2018.8352171.
2. Chowdhuri, S.; Mukherjee, A. An evolutionary approach to optimize speed controller of DC machines. In Proceedings of the Proceedings of IEEE International Conference on Industrial Technology 2000, 2000, Vol. 1, pp. 682–687 vol.2. https://doi.org/10.1109/ICIT.2000.854251.
3. Bostani, Y. Speed Control of DC Motor Using Extended Kalman FilterBased Fuzzy PID. *International Journal of Information and Electronics Engineering* **2013**. https://doi.org/10.7763/IJIEE.2013.V3.277.
4. Huang, G.; Lee, S. PC-based PID speed control in DC motor. In Proceedings of the 2008 International Conference on Audio, Language and Image Processing, 2008, pp. 400–407. https://doi.org/10.1109/ICALIP.2008.4590052.
5. Thorat, M.A.A.; Yadav, S.; Patil, S.S. Implementation of Fuzzy Logic System for DC Motor Speed Control using Microcontroller. *International Journal of Engineering* **2013**, *3*.
6. Rai, J. Speed Control of Dc Motor Using Fuzzy Logic Technique. *IOSR Journal of Electrical and Electronics Engineering* **2012**, *3*, 41–48. https://doi.org/10.9790/1676-0364148.

 doi:10.20944/preprints202605.0603.v1

7. Deshpande, P.; Deshpande, A. Inferential control of DC motor using Kalman Filter. In Proceedings of the 2012 2nd International Conference on Power, Control and Embedded Systems, 2012, pp. 1–5. https://doi.org/10.1109/ICPCES.2012.6508056.
8. Jayetileke, H.R.; de Mei, W.R.; Ratnayake, H.U.W. Real-time fuzzy logic speed tracking controller for a DC motor using Arduino Due. In Proceedings of the 7th International Conference on Information and Automation for Sustainability, 2014, pp. 1–6. ISSN: 2151-1810, https://doi.org/10.1109/ICIAFS.2014.7069560.
9. Abut, T. Modeling and Optimal Control of a DC Motor. *International Journal of Engineering Trends and Technology (IJETT) ISSN:2231-5381* **2016**, *32*, 146–150. https://doi.org/10.14445/22315381/IJETT-V32P227.
10. Cardona Soto, J.A.; Ponce, I.U.; Soto, I.; García, M.A.; Mejía, G. Identification of Dynamic Parameters in a DC Motor Using Step and Ramp Torque Response Methods. *Sensors* **2026**, *26*, 78. https://doi.org/10.3390/s26010078.
11. Popov, N. NON-LINEAR MODEL IN REGION OF VERY LOW SPEEDS FOR A PERMANENT MAGNET DIRECT CURRENT MOTOR. *ENVIRONMENT. TECHNOLOGY. RESOURCES. Proceedings of the International Scientific and Practical Conference* **2024**, *3*, 225–231. https://doi.org/10.17770/etr2024vol3.8152.
12. Rigatos, G.G.; Siano, P. Sensorless Control of Electric Motors with Kalman Filters: Applications to Robotic and Industrial Systems. *International Journal of Advanced Robotic Systems* **2011**, *8*, 71. https://doi.org/10.5772/10680.
13. Rigatos, G.G. Adaptive fuzzy control of DC motors using state and output feedback. *Electric Power Systems Research* **2009**, *79*, 1579–1592. https://doi.org/10.1016/j.epsr.2009.06.007.
14. Almatheel, Y.A.; Abdelrahman, A. Speed control of DC motor using Fuzzy Logic Controller. In Proceedings of the 2017 International Conference on Communication, Control, Computing and Electronics Engineering (ICCCCEE), 2017, pp. 1–8. https://doi.org/10.1109/ICCCCEE.2017.7867673.
15. Pirani, Y.; Salehfar, H.; Kumaran, J.S.; Ranganathan, P. Fuzzy Logic-based PMDC Motor Speed Control. In Proceedings of the 2025 57th North American Power Symposium (NAPS), 2025, pp. 1–6. ISSN: 2833-003X, https://doi.org/10.1109/NAPS66256.2025.11272263.
16. Abdulhussein, K.G.; Yasin, N.M.; Hasan, I.J. Comparison of cascade P-PI controller tuning methods for PMDC motor based on intelligence techniques. *12*, 1–11. https://doi.org/10.11591/ijece.v12i1.pp1-11.
17. Abdulhussein, K.G.; Yasin, N.M.; Hasan, I.J. Position - Velocity Control for Two PMDC Motors Connected by a Cross-Coupling Technique with Butterflies Optimization Algorithm. *3*, 31–44. https://doi.org/10.51173/jt.v3i2.323.
18. Guntay, S.; Saritas, I. BLDC Motor speed control with dynamic adjustment of PID coefficients: Comparison of fuzzy and classic PID. *12*, 22–32. https://doi.org/10.58190/ijamec.2023.80.
19. Karboua, D.; Toual, B.; Mosaad, M.I.; Youcef, C.; Bengharbi, A.A.; Hussien, S.A. Performance enhancement of PMSM using a hybridizing of nonlinear backstepping control and an optimized linear quadratic regulator. *43*, 2637–2664. https://doi.org/10.1177/01445987251353243.
20. Kızmaz, H. Comparative Analysis of Optimal Control Strategies: LQR, PID, and Sliding Mode Control for DC Motor Position Performance. *10*, 571–592. https://doi.org/10.54287/gujsa.1393092.
21. Afifa, R.; Ali, S.; Pervaiz, M.; Iqbal, J. Adaptive Backstepping Integral Sliding Mode Control of a MIMO Separately Excited DC Motor. *12*, 105. https://doi.org/10.3390/robotics12040105.
22. Omeje, C.O.; Salau, A.O.; Eya, C.U. Dynamics analysis of permanent magnet synchronous motor speed control with enhanced state feedback controller using a linear quadratic regulator. *10*, e26018. https://doi.org/10.1016/j.heliyon.2024.e26018.
23. Nguyen, T.H.; Nguyen, T.T.; Minh Le, K.; Tran, H.N.; Jeon, J.W. An Adaptive Backstepping Sliding-Mode Control for Improving Position Tracking of a Permanent-Magnet Synchronous Motor With a Nonlinear Disturbance Observer. *11*, 19173–19185. https://doi.org/10.1109/ACCESS.2023.3248604.
24. Chalardsakul, T.; Piliyasilpa, C.; Sukontanakarn, V. TMS320F28379D microcontroller for speed control of permanent magnet direct current motor. *IAES International Journal of Artificial Intelligence (IJ-AI)* **2024**, *13*, 2816–2828. https://doi.org/10.11591/ijai.v13.i3.pp2816-2828.
25. Yetayew, T.T.; G/Meskel, T.G.; G/michael, D.M. A Concise Evaluation of Auto-tuned PID and Fuzzy Logic Controllers for Speed Control of a DC-Motor. In Proceedings of the Advances of Science and Technology, Cham, 2022; pp. 256–268. https://doi.org/10.1007/978-3-030-93709-6_17.
26. Gubara, W.; Elnaim, M.; Babiker, S.F. Comparative study on the speed of DC motor using PID and FLC. In Proceedings of the 2016 Conference of Basic Sciences and Engineering Studies (SGCAC), 2016, pp. 24–29. https://doi.org/10.1109/SGCAC.2016.7458001.

 doi:10.20944/preprints202605.0603.v1

27. Pandey, V.D.; Giri, V. Comparative Analysis of Different Speed Control Methods for DC Drives. 2025. Pages: 50, https://doi.org/10.64289/rericproc.25.0105.4618368.
28. Raza, W.; Adzikya, D.; Mehmood, D.S.; Wasti, S.; Hussain, M.; Ahmad, A.; Usman, M.; Raza, S. Fuzzy Logic Speed Regulator for D.C. Motor Tuning. *JTAM (Jurnal Teori dan Aplikasi Matematika)* **2024**, *8*, 36. https://doi.org/10.31764/jtam.v8i1.16919.
29. Shieh, R.; Lu, Y.S. Jerk-constrained time-optimal control of a positioning servo. In Proceedings of the ICCAS 2010, 2010, pp. 1473–1476. https://doi.org/10.1109/ICCAS.2010.5670139.
30. Li, H.; Gong, Z.; Lin, W.; Lippa, T. Motion profile planning for reduced jerk and vibration residuals **2007**. https://doi.org/10.13140/2.1.4211.2647.
31. Rew, K.H.; Ha, C.W.; Kim, K.S. A practically efficient method for motion control based on asymmetric velocity profile. *International Journal of Machine Tools and Manufacture* **2009**, *49*, 678–682. https://doi.org/10.1016/j.ijmachtools.2009.01.008.
32. Rivera, D.E.; Morari, M.; Skogestad, S. Internal model control: PID controller design. *Industrial & Engineering Chemistry Process Design and Development* **1986**, *25*, 252–265. https://doi.org/10.1021/i200032a041.
33. Yetayew, T.T.; G/Meskel, T.G.; G/michael, D.M. A Concise Evaluation of Auto-tuned PID and Fuzzy Logic Controllers for Speed Control of a DC-Motor. In Proceedings of the Advances of Science and Technology; Berihun, M.L., Ed., Cham, 2022; pp. 256–268. https://doi.org/10.1007/978-3-030-93709-6_17.
34. Savitzky, A.; Golay, M.J.E. Smoothing and Differentiation of Data by Simplified Least Squares Procedures. *Analytical Chemistry* **1964**, *36*, 1627–1639. https://doi.org/10.1021/ac60214a047.